INTERNATIONAL JOURNAL of RENEWABLE ENERGY RESEARCH
X. Cao, Vol.16, No.2, June, 2026

P2P Energy Trading Based on Multi Objective NSGA-II for Pollution Reduction and Social Welfare Enhancing Considering RES Uncertainty Model

Xiao Cao*

*Department of Mathematics, Xinzhou Normal University, Shanxi Xinzhou 034000, China

‡Corresponding Author; Xiao CAO, cxlxy0204@163.com

Received: 29.12.2025 Accepted: 02.02.2026

Abstract- This study presents an advanced peer-to-peer energy trading framework that integrates renewable energy source uncertainty modeling, demand response, and multi-objective optimization using the Non-dominated Sorting Genetic Algorithm II (NSGA-II). The proposed approach aims to minimize carbon dioxide emissions while maximizing social welfare within a decentralized microgrid network. Uncertainties in photovoltaic irradiance, wind speed, and load demand are modeled using lognormal, Weibull, and normal probability density functions, respectively. A recurrent neural network is employed to forecast baseline day ahead renewable generation and demand profiles, providing accurate temporal data for optimization. The fitted distributions are then used to represent uncertainty around these baseline forecasts for scenario construction. The simulated system comprises 60 participants, including 20 prosumers and 40 consumers, equipped with photovoltaic units, wind turbines, battery energy storage systems, and electric vehicles. Two operational scenarios are examined: a baseline case without DR and an enhanced case including DR. In the baseline scenario, the optimal solution achieves a social welfare index of $6721.449 and total emissions of 3255.172 kg CO_2. When DR is implemented, emissions are reduced by approximately 17.3%, while welfare decreases by about 14.6 %, revealing a clear environmental-economic trade-off. Pareto front analysis confirms that demand response participation effectively reduces demand peaks, improves renewable energy utilization, and lowers reliance on diesel generators. Overall, the NSGA-II-based P2P trading and DR coordination framework enhances sustainability, flexibility, and robustness under renewable uncertainty. The proposed model provides a scalable decision-support tool for emission-conscious and welfare-optimized smart grid communities, supporting efficient integration of distributed energy resources in low-carbon electricity markets worldwide.

Keywords Peer-to-peer energy trading, uncertainty modeling, coordinated demand response, non-dominated sorting genetic algorithm II, recurrent neural network, social welfare.

1. Introduction

The fast decentralization of the power sector, driven by advances in DER and renewable energy systems, has changed traditional power networks into complex and dynamic ecosystems [1], [2]. P2P energy trading has become a transformative model that gives an opportunity to prosumers to directly exchange surplus energy with consumers. This action reduces dependence on centralized utilities [3]. The integration of variable renewable sources, such as PV and wind energy, introduces substantial operational uncertainty and poses challenges for grid stability and market efficiency [4], [5]. Moreover, greater demand-side participation via DR introduces behavioral complexity to local markets, where individual decisions affect collective outcomes [6], [7]. Multi-objective optimization methods, particularly evolutionary algorithms like NSGA-II, provide powerful tools for balancing conflicting goals such as emission minimization, cost reduction, and social welfare maximization [8], [9], [10]. At the same time, advances in machine learning, especially

RNNs, enable more accurate forecasting of stochastic renewable generation and load variations, strengthening the reliability of decentralized trading models [11], [12]. Within this context, the present study develops a comprehensive NSGA-II-based P2P trading framework that integrates RES uncertainty modeling, coordinated DR participation, and RNN-based forecasting as baseline day-ahead trajectories to jointly optimize environmental and economic performance in a decentralized microgrid environment. The main objective of this study is to reduce total emissions and increase social welfare under renewable uncertainty, supporting an extendable decision-support model for the emission-aware and welfare-oriented smart energy communities.

2.1. Literature Review

Uddin et al. [13] proposed an optimized decentralized P2P energy trading scheme for smart grids to mitigate challenges caused by renewable-energy uncertainty. Fuzzy optimization technique was adapted to inherent variability in renewable generation, with the objective of improving the effectiveness of decentralized energy systems. The proposed model reduced operating costs and improved reliability. Simulation results indicated that the fuzzy approach outperformed conventional methods by providing a more cost-effective and dependable P2P trading solution under uncertainty. Xie and Li [14] investigated P2P energy trading in interactive communities using a two-stage optimization framework. The initial stage balanced individual and community benefits to determine user participation, while the second stage improved economic performance through a payment negotiation mechanism. A case study reported cost reductions, enhanced adoption of renewable energy, and higher profits for the participants. The research emphasized the efficacy of Nash bargaining theory and privacy-preserving algorithms in enhancing social welfare. however, the study focused mainly on wind energy and adopted simplified energy-storage assumptions. Al-Abri et al. [15] investigated a P2P energy trading model that incorporates Greenhouse Gas (GHG) reduction to support a sustainable transition in energy for Oman. A decentralized framework employing GHG credits was suggested to enable energy exchanges among prosumers and consumers. The model used an NSGA-II to prosumer profit, consumer cost, and penalties associated with power loss, under investment-based cost, and greenhouse gas allowance constraints. Case studies using the IEEE 14-bus system with Omani grid data showed that the framework improved social welfare, trade efficiency, and system resilience under diverse operational conditions. Dai and Batool [16] tackled the global warming crisis by creating an interactive energy-sharing network that incorporates electrochemical battery storage within multi-energy district systems. The study emphasized modeling battery degradation using an intelligent system for managing energy and applying multi-criteria decision analysis. A Monte Carlo Tree Search integrated with a multi-criteria optimization method was utilized for effective energy coordination. The framework applies both deterministic and stochastic techniques for handling weather and demand uncertainty, while machine learning models are used to predict battery degradation more accurately than traditional models. Results showed a rise in renewable energy adoption, more stable demand, and enhanced microgrid resilience. Yavuz and Kivanc [17] investigated P2P energy trading, which is integrated with Vehicle-to-X (V2X) technologies, including V2H, V2L, and V2G. The study aimed to improve the prosumer participation and also enhance their flexibility for energy usage. They proposed an Energy Management System (EMS) by using a Deep Reinforcement Learning (DRL), so pricing strategies and processes for exchanging energy may be optimized while the comfort of the prosumer can be maintained. Use of Multi Double Deep Q-Network (DDQN) agents under a Markov Decision Process (MDP) framework allowed their model to achieve 19.18% cost reduction, a 9.39% increase in the Self-Sufficiency Ratio (SSR), and showed that effective management of energy uncertainties could be realized in cluster-based P2P networks. Karthik et al. [18] proposed a Chaotic Self-Adaptive Sine Cosine Algorithm (CSASCA) for addressing the multi-objective scheduling issue in microgrids, aiming to reduce the costs and emissions. The research used fuzzy logic to increase decision-making accuracy and produced the best solutions, which balanced economic and environmental goals effectively. The algorithm outperformed conventional Sine Cosine Algorithm (SCA) in three testing situations. The results showed a better performance for operational costs, emission reduction, and execution time, giving an opportunity to demonstrate that the CSASCA enabled a quicker convergence, improved the constraint management, and provided higher optimization precision. Zhou [19] presented a dynamic self-learning grid-responsive technique for district buildings and vehicles interaction energy networks to improve techno-economic performance, energy flexibility, and battery capacity retention. The model incorporated building PV and EV within a collaborative multi-energy framework, accounting for the cycling degradation of both stationary and mobile batteries. The strategy employed multi-objective optimization and a weighted Eulerian distance-based decision procedure, resulting in a reduction in import costs from 213.2 to 203.8 HK$/m²·a and an enhancement of relative capacity from 0.800 to 0.999, which demonstrated its efficacy in smart district energy networks. Akiyamaya and Shinomiya [20] investigated the P2P energy trading model as a substitute for the Feed-in Tariff (FIT) system, focusing on its economic constraints and sustainability issues. They presented an optimization-centric framework to enhance market efficiency and equity by optimizing transaction partners and trading volumes among households. Efficiency was defined as reduced resource wastage, while fairness intended to inhibit monopolistic practices. The study, using simulated tests comparing single- and multi-objective optimization, determined that the latter is more effective in improving market performance and participant equity in P2P electricity trading. Gao et al. [21] acknowledged limitations in centralized trading frameworks inside a Multi-Microgrid (MMG) system. They then developed and distributed a robust operational strategy that uses P2P multi-energy trading. Their research shows a two-stage robust optimization (TRO) framework for dealing with uncertainties of renewable energy and loads, using the Nash bargaining theory to support fair cooperation among involved microgrids. A distributed algorithm maintains data privacy throughout trade activities. Simulation outcomes involving three microgrids validated that the proposed technique

enhanced fairness, energy efficiency, and cooperation while ensuring supply reliability in the face of unpredictability. Lokesh and Badar [22] developed a multi-objective optimization model for networked microgrids to ascertain the optimal dimensions of RES and BESS. The research introduced proportional P2P and a P2G energy trading framework, which is managed by a microgrid aggregator. By applying a Multi-Objective Particle Swarm Optimization (MOPSO), the research planned to lower the annual energy expenditure and the probability of supply interruptions as well. The outcomes showed reduced grid interaction, better use of renewables, and a notable reduction in the BESS capacity, which gives an improvement in economic and system reliability performance.

Table 1 provides a concise feature-level comparison of representative studies from the literature review in relation to the present work.

Table 1. Feature-level comparison of representative studies and this work

Ref.	P2P	DR	Uncertainty	ML Forecast	Emis. Obj.	NSGA-II	EV/V2G
[13]	✓	✗	✓	✗	✗	✗	✗
[14]	✓	✗	✗	✗	✗	✗	✗
[15]	✓	✗	✗	✗	✓	✓	✗
[16]	✓	✗	✓	✓	✓	✗	✗
[17]	✓	✗	✓	✗	✗	✗	✓
[18]	✗	✗	✗	✗	✓	✗	✗
[19]	✗	✗	✗	✗	✓	✗	✓
[20]	✓	✗	✗	✗	✗	✗	✗
[21]	✓	✗	✓	✗	✗	✗	✗
[22]	✓	✗	✗	✗	✗	✗	✗
Study	✓	✓	✓	✓	✓	✓	✓

2.2. Research Gap and Innovations

Despite fast advancements in P2P energy trading, numerous gaps remain when markets are implemented in renewable-abundant localities. Numerous existing studies focus on economic performance or environmental objectives in isolation, whereas the combined assessment of emission-welfare trade-offs under renewable variability remains constrained. Moreover, uncertainty is frequently depicted through oversimplified assumptions that inadequately capture the impact of temporal fluctuations in photovoltaic generation, wind output, and load demand on market results. Furthermore, demand response is often regarded as an external modification or a generic flexibility asset, rather than being integrated into the market model in a manner that explicitly considers its welfare consequences.

In response to these deficiencies, this paper formulates a comprehensive P2P trading framework that integrates uncertainty representation, temporal forecasting, coordinated demand response, and multi-objective optimization into a unified decision-support workflow. This work's unique contributions are summarized as follows:

- Integrated P2P–uncertainty–forecasting workflow:

The framework integrates peer-to-peer trading with renewable/load variability by modeling photovoltaic irradiance, wind speed, and demand uncertainty through probabilistic distributions and generating scenario realizations around the baseline forecasts for operational analysis.

- Time-resolved, data-driven inputs:

An RNN is employed to predict hourly photovoltaic, wind, and demand profiles, offering time-varying inputs for scheduling instead of static deterministic patterns.

- Coordinated demand response with welfare accounting:

Demand response is structured through an incentive–discomfort framework, allowing for the precise measurement of the welfare effects of flexibility participation in conjunction with emission results.

- Scenario-based Pareto trade-off assessment:

A multi-objective formulation based on NSGA-II produces Pareto-optimal emission-welfare solutions, which are compared between scenarios with and without demand response.

- Community-scale validation with heterogeneous resources:

The model is assessed within a hybrid prosumer-consumer community featuring photovoltaic and wind generation, battery storage, electric vehicles (both residential and commercial), auxiliary diesel generation, and grid interaction to evaluate trading and dispatch results under coordinated flexibility.

3. Methodology

The suggested P2P energy trading framework incorporates renewable energy uncertainty modeling, RNN forecasting, and multi-objective optimization through NSGA-

II to realize a sustainable, welfare-optimized smart grid. Fig. 1 shows a system that includes several prosumers equipped with PV panels, WTs, a BESS, and EVs. These prosumers are linked with consumers, DG, an EV charging station, and the main electrical grid. The uncertainties associated with solar irradiance, wind speed, and load demand are being modeled by lognormal, Weibull, and normal PDFs, respectively. The RNN model forecasts baseline day-ahead generation and demand trajectories, providing reliable temporal data for optimization. The fitted PDFs are used to characterize uncertainty around the baseline forecasts for scenario construction. NSGA-II subsequently identifies Pareto-optimal solutions that balance emission reduction and social welfare enhancement under two operational scenarios.

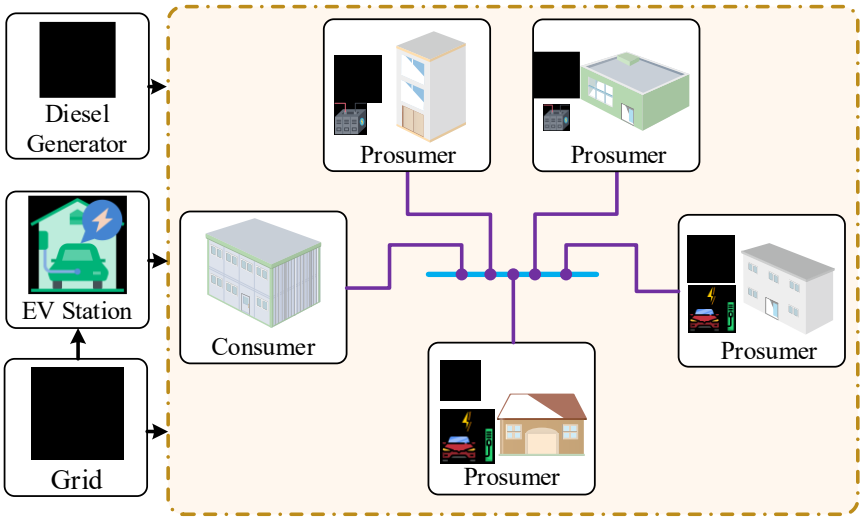

Fig. 1. The proposed P2P energy trading framework.

3.1. Uncertainty Modeling

The Continuous probability density functions are used to characterize uncertainty sources in irradiance, wind speed, and load demand, and to generate stochastic realizations around the baseline forecasts for scenario-based analysis [23].

3.1.1. PV modeling

Also, a lognormal PDF gives an opportunity to characterize the uncertainty that exists in solar irradiance.

$$f_G(g) = \frac{1}{g\sigma_s\sqrt{2\pi}} \exp\left[-\frac{(\ln G - \mu_s)^2}{2{\sigma_s}^2}\right] \text{ for } g > 0, \quad (1)$$

Here, σ_s and μ_s denote the standard deviation and mean of the random variables, assigned values of 5.5 and 0.5, respectively.

The PV output power as a function of irradiance is computed as:

$$P_s(G) = \begin{cases} P_{sr}\left(\dfrac{G^2}{G_{std} \times M_c}\right) & \text{for } 0 < G \le M_c \\ P_{sr}\left(\dfrac{G}{G_{std}}\right) & \text{for } G \ge M_c \end{cases} \quad (2)$$

Where M_c=120 W/m² is the specified irradiance point and $G_{\text{std}} = 1000\text{W/m}^2$. and G_n^{min} and G_n^{max} denotes the lower and upper bounds of irradiance in scenario n.

3.1.2. Wind turbine modeling

The changes in wind speed are represented through the Weibull PDF, which is shown in Eq. (3).

$$f_v(v) = \left(\frac{\beta}{\alpha}\right)\left(\frac{v}{\alpha}\right)^{(\beta-1)} \exp\left[-\left(\frac{v}{\alpha}\right)^{\beta}\right] 0 \le v < \infty. \quad (3)$$

The shape and scale parameters of the Weibull PDF, known as an β and α, were determined as $\beta = 2.6$ and $\alpha = 10.5$.

The power output produced from WT depends on the wind velocity, and it can be stated through the relation indicated in Eq. (4):

$$P_\omega(v_\omega) = \begin{cases} 0 & \text{for } v_\omega < v_{\omega i} \mid v_\omega > v_\omega \\ P_{\omega r}\left(\dfrac{v_\omega - v_{\omega i}}{v_{\omega r} - v_{\omega i}}\right) & \text{for } (v_{\omega i} \le v_\omega \le v_{\omega r}) \\ P_{\omega r} & \text{for } (v_{\omega r} \le v_\omega \le v_{\omega v}) \end{cases}, \quad (4)$$

where $P_{\omega r}$ is the rated output power of the WT, and $v_{\omega i} = \frac{3\text{ m}}{\text{s}}$, $v_{\omega 0} = \frac{25\text{ m}}{\text{s}}$, and $v_{\omega r} = \frac{16\text{ m}}{\text{s}}$ are the cut-in, cut-out, and rated speed of the WT, respectively.

3.1.3. Load demand modeling

As it is presented in Eq. (5), the PDF of the normal distribution can be employed to model the load demand uncertainty:

$$f_d(P_d) = \frac{1}{\sigma_d\sqrt{2\pi}} \exp\left[-\frac{(P_d - \mu_d)^2}{2{\sigma_d}^2}\right], \quad (5)$$

The terms σ_d and μ_d represent standard and mean deviations, respectively. P_d refers to the probability density for the load's normal distribution.

3.2. Diesel Generator

When RES, together with the battery bank, cannot fulfill the load power requirement, DG acts as an auxiliary supply for power. The hourly usage of fuel for a DG can be determined by using Eq. (6) [24].

$$F_{DG}(t) = \alpha P_{DG}(t) + \beta P_r \quad (6)$$

Where the fuel intake rate $F_{DG}(t)$ is measured in L/hr, the instantaneous power generation $P_{DG}(t)$ is given in kW, the nominal generator capacity P_r is expressed in kW, α indicates the fuel curve slope coefficient and β refers to the fuel intercept coefficient. The parameters α and β utilized in this investigation are defined as α=0.246 and β=0.08415 [25]

The DG's efficacy can be computed as shown in Eq. (7):

$$\eta_{\text{overall}} = \eta_{\text{brake-thermal}} \times \eta_{\text{generator}} \quad (7)$$

Where $\eta_{\text{overall}}, \eta_{\text{generator}}$, and $\eta_{\text{brake-thermal}}$ signifies the total, generator, and brake thermal efficiencies of the DG, respectively.

The optimization model integrates the operational and technological limitations of the DG to guarantee realistic functionality and dependability.

The output power of the DG is constrained by its lowest and maximum generating thresholds in Eq. (8):

$$P_{DG}^{min} \leq P_{DG}(t) \leq P_{DG}^{max} \quad (8)$$

3.3. Battery Energy Storage System

The BESS constraints are given in Eqs. (9-14) [22]:

$$0 \leq E_{\text{e}} \leq E_{\text{e,max}} \quad (9)$$

$$0 \leq P_t^{\text{ch}} \leq u_t^{\text{ch}} P_{\text{ch,max}} \quad (10)$$

$$0 \leq P_t^{\text{dis}} \leq u_t^{\text{dis}} P_{\text{dis, max}} \quad (11)$$

$$E_{\text{e},t} = E_{\text{e},t-1} + \eta_{\text{e,ch}} P_t^{\text{ch}} \Delta t - P_t^{\text{dis}} \Delta t / \eta_{\text{e,dis}} \quad (12)$$

$$E_{\text{e, T}} = E_{\text{e,0}} \quad (13)$$

$$u_t^{\text{ch}} + u_t^{\text{dis}} \leq 1 \quad (14)$$

where $E_{\text{e},t}$ is the stored energy of the BESS e at time t (kWh), P_t^{ch} and P_t^{dis} denote the charging and discharging power (kW), $P_{\text{ch,max}}$ and $P_{\text{dis, max}}$ are the maximum charging/discharging power limits (kW), u_t^{ch} and u_t^{dis} are binary variables indicates the charging and discharging states, $\eta_{\text{e,ch}}$ and $\eta_{\text{e,dis}}$ are charging/discharging efficiencies and Δt is the time step (1 h). Eq. (17) enforces a cyclic terminal condition, and Eq. (18) prevents simultaneous charging and discharging. For reporting and constraint interpretation, the state of charge is defined as follows in Eq. (15):

$$SoC_{e,t} = \frac{E_{e,t}}{E_{max}} \quad (15)$$

3.4. Electrical Vehicle

This study models EVs to function in two separate modes as follows:

3.4.1. EV home

The aim of the EV charging schedule is to maximize comfort for homeowners while minimizing the costs of charging by using a dynamic power pricing strategy. The EV's charging needs to be scheduled for when it arrives and leaves according to the home's EMS. As indicated in Eqs. (16-20), the following are the limitations of EV charging planning and the state transition function [26]:

$$SOC_t^{EV} = \begin{cases} SOC_{t-1}^{EVh} + E_{t-1}^{EVh}, \text{if } t \leq t_{de} \text{ or } t > t_{ar} \\ SOC_{ar}, \text{if } t = t_{de} \end{cases} s.t \quad (16)$$

$$0 \leq SOC_t^{EVh} \leq SOC_{max}^{EVh} \quad (17)$$

$$0 \leq E_t^{EVh} \leq E_{\text{max}}^{EVh} \quad (18)$$

$$SOC_{t_d}^{EVh} \geq SOC_{\text{target}}^{EVh} \quad (19)$$

$$E_t^{EVh} = 0, \text{if } t \in [t_{de}, t_{ar}) \quad (20)$$

Here, t_{ar} and t_{de} denotes the arrival and departure hours of EVh, respectively. The EV is available for charging during $t \in [t_{de}, t_{ar})$, outside this interval $E_t^{EVh} = 0$. E_t^{EVh} denotes the scheduled charging energy in hour t (kWh) with $\Delta t = 1h$.

3.4.2. EV station

EV stations function as collective charging points that coordinate several EVs for charging and Vehicle-to-Grid (V2G) activities. Their scheduling system plans to reduce overall energy expenses and also seeks a balance of local generation and demand within a P2P energy trading mechanism. In contrast with residential EVs, station-level management supervises simultaneous charging as well as discharging among several vehicles. Eqs. (21-25) operational constraints are governing EV station participation in the optimization process:

$$SOC_{EV,st}^{\min} \leq SOC_{EV,st}(t) \leq SOC_{EV,st}^{\max} \quad (21)$$

$$0 \leq P_{EV,st}^{ch}(t) \leq P_{EV,st}^{max,ch} \quad (22)$$

$$0 \leq P_{EV,st}^{dis}(t) \leq P_{EV,st}^{max,dis} \quad (23)$$

$$\delta_{EV,st}^{ch}(t) + \delta_{EV,st}^{dis}(t) \leq 1 \quad (24)$$

$$P_{EV,st}^{net}(t) = P_{EV,st}^{ch}(t) - P_{EV,st}^{dis}(t) \quad (25)$$

These constraints ensure the EV station operates within safe state-of-charge limitation, avoids charging and discharging at the same time, and keeps consistent energy transfer with the grid. Integration into an NSGA-II method gives the opportunity to optimize the cost, the welfare, and emission goals jointly in a P2P community.

3.5. Peer to Peer

P2P trading framework. This study characterizes P2P trade as localized energy exchanges among community participants over a 24-hour period. At each hour h, users may

participate in buying or selling energy through P2P transactions, constrained by feasible restrictions. Market clearing is achieved by mandating that the total peer-to-peer energy sold equals the total P2P energy purchased within the community for each hour. The resultant net P2P exchange for each participant is directly incorporated into the hourly power-balance restrictions alongside renewable energy, storage/EV charging and discharging, grid import, and diesel generation. Settlement payments are classified as internal transfers; hence, they do not influence the overall system welfare, which solely accounts for net operating costs/benefits and the demand response comfort-disutility term [27].

3.6. Coordinated Demand Response and Peer-To-Peer Energy Trading

This section defines the behavioral and coordination framework of the proposed decentralized optimization model, integrating demand-side flexibility with P2P energy trading to improve system welfare and reduce emissions. Each participant (consumer or prosumer) independently modifies its consumption or generation based on a locally established incentive signal within the P2P coordination framework. The modified net loads and surplus energy are then traded between peers, facilitating self-sufficient balancing and energy redistribution without a central authority. This decentralized framework captures the relationship between individual flexibility choices and system-level goals, providing the basis for operational scenarios investigated in this study, both with and without DR.

3.6.1. Demand-response formulation

Consumer discomfort caused by load curtailment is modeled through an exponential disutility function scaled by a monetary coefficient κ_j^h in Eq. (26) [28]:

$$\psi_j^h = \kappa_j^h \left(\exp\left[\beta_j \frac{PNS_j^h}{P_j^h} \right] - 1 \right) \tag{26}$$

Where P_j^h is the baseline demand (kW) of the consumer j at hour h; PNS_j^h is the curtailed portion; and $\beta_j > 0$ represents the consumer's discomfort sensitivity.

The system's profit from DR participation is formulated in Eq. (27) as the avoided marginal supply cost minus incentive payments distributed within the community:

$$C = \sum_{j=1}^{J} (m^h - \gamma^h) PNS_j^h \tag{27}$$

Where m^h denotes the marginal avoided cost (e.g., grid import price a^h or DG costc_{DG}^h), and γ^h represents the locally determined incentive rate (\$/kWh). The individual consumer benefit is expressed in Eq. (28):

$$CB_j^h = \gamma^h PNS_j^h - \psi_j^h \tag{28}$$

Consumers participate only if $CB_j^h \geq 0$, ensuring rational economic behavior. Feasibility and incentive constraints are given by Eqs. (29-32):

$$0 \leq PNS_j^h \leq \eta_j^h P_j^h \tag{29}$$

$$0 \leq \eta_j^h \leq 1 \tag{30}$$

$$0 \leq \gamma^h \leq m^h \tag{31}$$

$$\sum_j \gamma^h PNS_j^h \leq B^h \tag{32}$$

3.6.2. Optimal curtailment decision

For a given incentive signal γ^h, each consumer determines the optimal curtailed load PNS_j^{h*} by maximizing its net benefit ($\gamma^h PNS_j^h - \psi_j^h$). The corresponding first-order condition is:

$$\frac{d\psi_j^h}{dPNS_j^h} = \frac{\kappa_j^h \beta_j}{P_j^h} \exp\left(\beta_j \frac{PNS_j^h}{P_j^h} \right) = \gamma^h \tag{33}$$

To ensure reproducibility of the incentive feasibility and comfort-response settings, the numerical study adopts explicit DR parameter values. The comfort-sensitivity coefficient is set as $\beta_j \in \{1,2,3\}$ to represent low/medium/high discomfort sensitivity (consistent with incentive-based residential DR studies), and the monetary scaling is fixed to $\kappa_j^h = 1\$$ (monetary units). The incentive rate is constrained to $\gamma^h \in [0, 0.18]$ \$/kWh, and the feasible curtailed portion is limited by $0 \leq PNS_j^h \leq 0.4\, P_j^h$ to avoid unrealistic curtailment levels [28].

Solving for PNS_j^{h*} gives the closed-form optimal curtailed load:

$$PNS_j^{h*} = \left[\frac{P_j^h}{\beta_j} \ln\left(\frac{\gamma^h P_j^h}{\kappa_j^h \beta_j} \right) \right]_0^{\eta_j^h P_j^h} \tag{34}$$

The result is constrained within the feasible range $[0, \eta_j^h P_j^h]$; if the logarithmic term is non-positive, $PNS_j^{h*} = 0$.

3.6.3. Welfare accounting and scenario integration

The total system welfare is formulated in Eq. (35):

$$\text{Welfare} = \text{Consumer Surplus} + \text{System Profit} - \sum_{j,h} \psi_j^h \tag{35}$$

Here h is the time index (hour) and j denotes a participant/prosumer. All welfare quantities are reported in monetary units (\$) (consistent with the tariff and incentive values), and welfare values represent the aggregated 24-h net welfare.

Here, Consumer Surplus represents the participant's net benefit from electricity consumption/trading, System Profit denotes the net operating profit of the system (e.g., revenues minus energy procurement/dispatch costs), and ψ_j^h is the comfort-disutility (user inconvenience) term associated with demand response at prosumer j and hour h.

Accordingly, P2P settlement payments are treated as internal transfers and do not change the total system welfare, ensuring that the welfare index reflects only net economic impacts and comfort disutility. Welfare can decrease under DR when the incremental comfort-disutility associated with enforced load redistribution outweighs the operational savings from lower-emission dispatch.

Two operational scenarios are considered:

Without DR: $\gamma^h = 0 \Rightarrow PNS_j^h = 0$ and with DR: γ^h and PNS_j^h are optimized under Eq. (34) a-d, to balance welfare and emission objectives.

The resulting net load, defined as ($P_j^h - PNS_j^h$), is subsequently used in the P2P coordination and emission-welfare analysis, ensuring full consistency between consumer flexibility, decentralized energy exchange, and overall system optimization.

3.7. Objective Functions

The optimization model simultaneously minimizes total system emissions and maximizes overall social welfare under renewable-generation and demand uncertainties in Eq. (36) and Eq. (37), respectively:

$$\text{Minimize:} F_1 = \sum_{t=1}^{T} \sum_{i=1}^{N} \text{Emission}_i\left(P_{i,t}\right) \tag{36}$$

$$\text{Maximize:} F_2 = \sum_{i=1}^{N} \sum_{t=1}^{T} \left(B_{i,t} - D_{i,t}\right) \tag{37}$$

$B_{i,t}$ and $D_{i,t}$ denote, respectively, the economic benefit (avoided marginal cost, incentive gains) and disutility (comfort loss) for the participant i at time t.

where $Emission_i(P_{i,t})$ represents the CO_2 emissions (kg CO_2) attributed to microgrid i at time t. In this study, emissions are computed from grid-import electricity and diesel generator production as

$$Emission_i(P_{i,t}) = \left(\alpha^{grid} P_{i,t}^{grid} + \alpha^{DG} P_{i,t}^{DG}\right)\Delta t \tag{38}$$

where $P_{i,t}^{grid}$ is the grid import power, $P_{i,t}^{DG}$ is DG power, $\Delta t = 1$h, and α^{grid} and α^{DG} are emission factors in kg CO_2/kWh.

The NSGA-II algorithm searches for Pareto-optimal solutions between F_1 and F_2, producing the emission welfare frontiers which are discussed in the results section.

To ensure comprehensive reproducibility, the entire set of technical and economic inputs, along with the complete optimization configuration, is provided in Tables 2 and 3.

Table 2. Technical & economic parameters

Category	Parameter	Value	Unit
Horizon /Agents	Scheduling horizon	24	h
Horizon /Agents	Number of agents/households	60	–
Battery	Energy capacity	30	kWh
	SOC bounds	10–90% of $Cmax_{ESS}$	kWh
Efficiency	Battery charge/ discharge	0.95	–
	DG efficiency	0.6	–
	P2P transaction efficiency	0.98	–
	DG emission factor	0.72393	kg/kWh
	Grid emission factor	0.92125	kg/kWh
Costs	Battery charge/ discharge cost	0.03	$/kWh
	DG marginal cost	0.077	$/kWh
	PV marginal cost	0.02864	$/kWh
	Wind marginal cost	0.02675	$/kWh
	P2P price	0.03	$/kWh

Table 3. NSGA-II settings

Setting	Value
Algorithm	NSGA-II
Population size	50
Generations	200
Random seed	30
History saving	True
Verbose	True
Crossover/Mutation	SBX (prob=0.9, η=15)

3.8. RNN Prediction Modeling

An RNN is a type of artificial neural network that is designed for dealing with sequential or time-dependent data. These deep learning models are frequently used to solve problems with ordinal or temporal structure. The output in the RNNs depends on previous elements in the sequence. Although upcoming events may influence the output of a certain order, unidirectional RNNs are unable to incorporate these events into their predictions [29]. The net inputs are X_n and the delay term z_n^{-1} which is defined in Eq. (39);

$$z_n^{-1} = f\left(w_{zn} z_{n-1}^{-1} + w_{xn} x_n + b\right) \tag{39}$$

Here, b denotes bias and f represents an activation function. Two main activation functions are the sigmoid and the hyperbolic tangent functions.

The sigmoid function is shown in Eq. (40);

$$f(x) = \frac{1}{1 + e^{(-x)}} \tag{40}$$

So, z_n^{-1} presented as Eq. (41);

$$z_n^{-1} = 1/(1 + \exp\left(-(w_{zn} z_{n-1}^{-1} + w_{xn} x_n + b)\right) \tag{41}$$

Eq. (42) defines the tangent hyperbolic activation function as follows:

$$h(x) = \frac{(e^{-x} - e^{-x})}{(e^{-x} + e^{-x})} \tag{42}$$

The outputs of the net y_n which is defined in Eq. (43);

$$y_n^- = \mathrm{h}\left(\mathrm{w_{yn}} \mathrm{z_{n-1}^{-1}} + \mathrm{b_y}\right) \tag{43}$$

This can be represented as Eq. (44):

$$y_n^- = \tanh\left(\mathrm{w_{yn}} \mathrm{z_{n-1}^{-1}} + \mathrm{b_y}\right) \tag{44}$$

Where $\mathrm{w_{yn}}$ is outputs weights and b_y is bias and h is the hyperbolic activation function, which is indicated in Eq. (3).

In this study, the results of the model use RMSE and MAE, which can be determined by Eq. (45) and Eq. (46) [30]:

$$MAE = \frac{1}{n} \sum_{i=1}^{n} (x_i - \hat{x}_i) \tag{45}$$

$$RMSE = \sqrt{\frac{1}{n} \sum_{i=1}^{n} (x_i - \hat{x}_i)^2} \tag{46}$$

Where n denotes the sample's total number, x_i and $\hat{x}_i$ defines the laboratory-measured and prediction output of the i^{th} sample, respectively.

The RNN has been trained on hourly demand, photovoltaic, and wind time series utilizing a chronological division of 70% for training, 15% for validation, and 15% for testing, without shuffling. Inputs have been normalized [31] by min-max scaling applied to the training subset. The model has been optimized using Adam with a learning rate of 0.001, a batch size of 32, and trained for 200 epochs, with early stopping based on validation loss. The forecasting performance is evaluated using MAE and RMSE on the reserved test set.

3.9. Uncertainty Propagation and Scenario Reduction

The RNN model provides the baseline day-ahead trajectories for PV, wind, and demand (Section 3.8). Uncertainty is propagated by generating SMonte-Carlo scenarios around the baseline profiles using the fitted distributions. For each hour t, scenario realizations are formed as follows in Eq. (47) [32]:

$$\tilde{x}_{t,s} = \hat{x}_t + \varepsilon_{t,s}, \varepsilon_{t,s} \sim \mathcal{D}_x, x \in \{D, PV, WT\} \tag{47}$$

where $\hat{x}_t$ denotes baseline forecast and $\mathcal{D}_x$ is the corresponding fitted distribution.

Scenario reduction/aggregation step is then applied, and representative input is taken as the scenario-mean profile as follows in Eq. (48):

$$\bar{x}_t = \frac{1}{S} \sum_{s=1}^{S} \tilde{x}_{t,s}, x \in \{D, PV, WT\} \tag{48}$$

NSGA-II is implemented as a day-ahead scheduling problem using the scenario-mean demand/PV/wind profiles as representative inputs, whereas the generated scenarios are used to quantify the variability around the baseline trajectories.

4. Numerical Result

The proposed simulation framework reveals a local energy community that consists of 40 consumers and 20 prosumers, categorized into four different types that show variety in the generation as well as flexibility of resources. Type 1 prosumers possess PV panels integrated with BESS, which provides daily load shifting and renewable self-consumption. Type 2 prosumers integrate PV systems with EV, providing increased flexibility by means of mobile energy storage and V2G capabilities. Type 3 prosumers integrate WTs with BESSs to ensure a consistent renewable energy supply and provide energy support during nighttime. Type 4 prosumers oversee WT operations across EV, coordinating variable generation with mobile storage flexibility. The twenty prosumers and forty consumers collectively establish a realistic micro-market environment for assessing the interaction between renewable variability, storage dynamics, and P2P energy exchanges. The diverse configuration offers an accurate assessment of emission and welfare performance in both demand-response and non-demand-response operational contexts.

4.1. Demand–Price Profile

Fig. 2 presents the hourly demand and electricity price profiles used in the numerical analysis. Demand remains low overnight, increases gradually during the day, and peaks around 20:00–21:00 (≈200kW). The time-of-use price follows a similar pattern, rising from about \$0.27/kWh during off-peak hours to about \$0.55/kWh at peak periods, which is consistent with typical market conditions where higher demand coincides with higher prices. These profiles are used as the main inputs for the subsequent emission–welfare assessments.

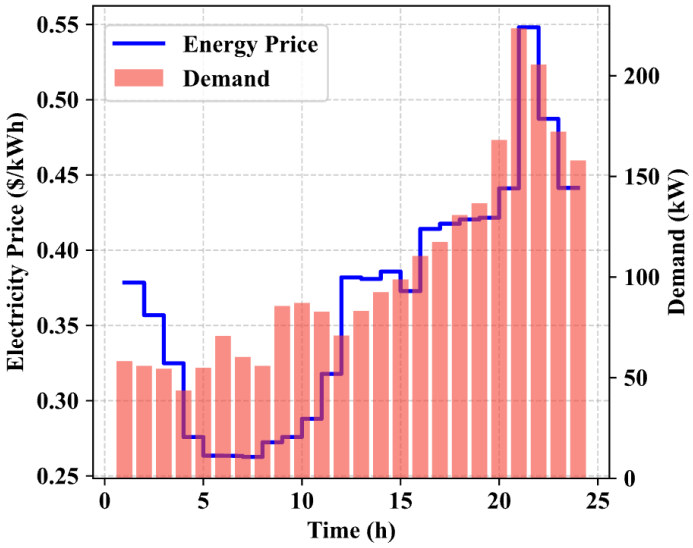

Fig. 2. Hourly electricity price and demand profiles over 24 h.

This daily demand–price coupling demonstrates that the machine learning-driven forecasting and NSGA-II-based market-clearing algorithm effectively replicates the temporal dynamics of supply–demand equilibrium, thereby establishing a credible basis for subsequent emission–welfare trade-off analysis.

4.2. Predicted Profiles of PV, Wind, and Demand with Uncertainty

Fig. 3 shows predicted hourly profiles of demand, PV power, and wind power produced by machine-learning models over a 24-hour horizon. Demand exhibits a distinct peak around 19:00 hours. PV generation follows a normal solar pattern, increases post-sunrise, reaches a high of around midday (about 23 kW), and declines to near zero at night. Wind power demonstrates higher variability, yielding comparatively higher outputs during the early morning and evening hours. The shaded bands denote the forecast uncertainty determined by model residual distributions, showing stochastic variations in load behavior. The uncertainty bounds are subsequently integrated into the scenario-based analysis to evaluate the resilience of emission and welfare outcomes under variable renewable conditions. To further illustrate how forecast uncertainty is represented, Figs. 4(a-c) report the generated scenario trajectories and the corresponding scenario-mean profiles for demand, PV power, and wind power over the 24-h horizon. In this study, $S = 30$ scenarios are generated, and the scenario spread and mean trajectories are reported for transparency.

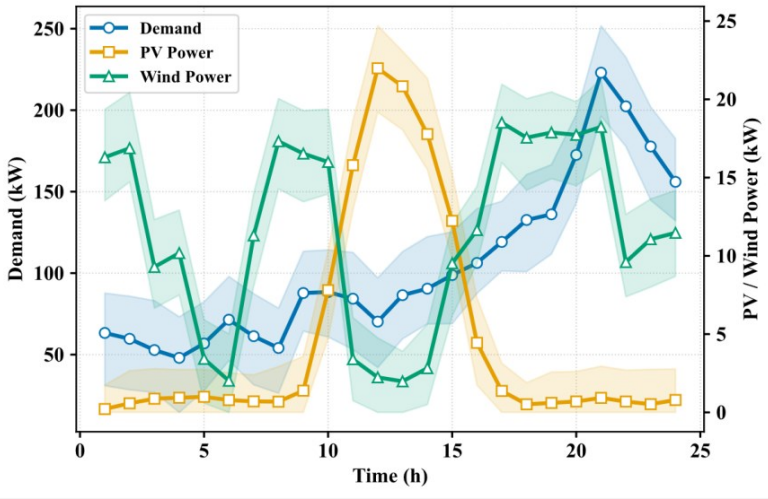

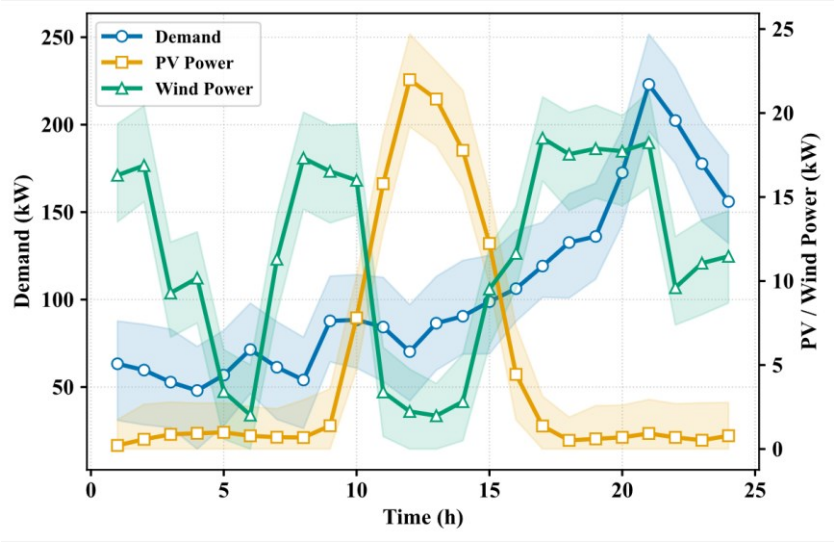

Fig. 3. Predicted hourly profiles of demand, PV generation, and wind generation with associated uncertainty ranges.

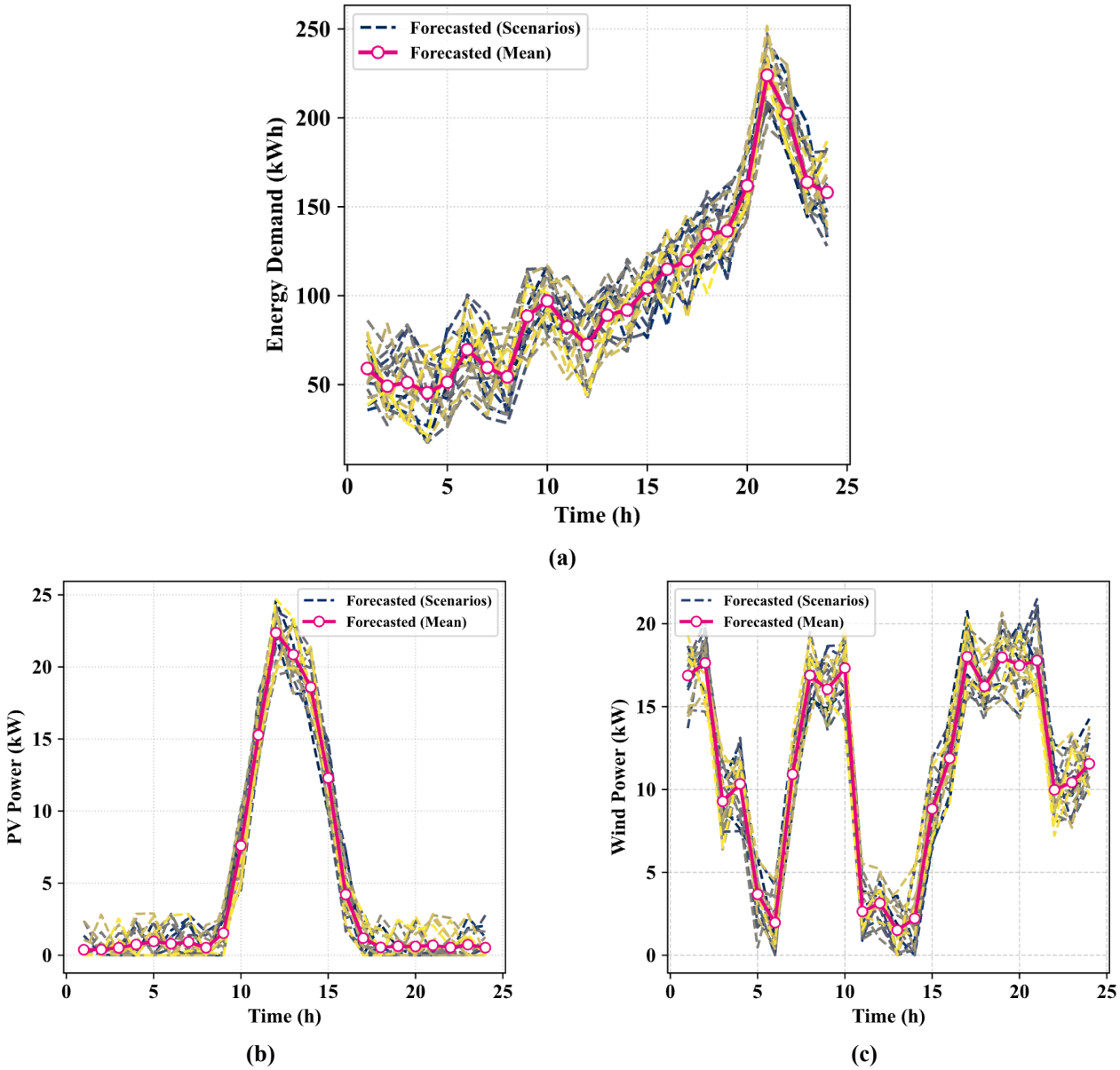

Fig. 4. Generated scenarios and the corresponding scenario-mean profile over the 24-h horizon.

4.3. Scenario 1: Without Demand Response

Fig. 5 depicts the patterns of P2P imports and exports over a 24-hour period. Imports are increasing significantly during the periods of high demand, reaching their highest point between 16:00 and 21:00 hours. In contrast, exports dominate midday when the PV output is greater than local consumption. The alternating flow emphasizes dynamic bilateral exchanges that reallocate surplus renewable energy to deficit agents, improving network utilization even in the absence of active DR.

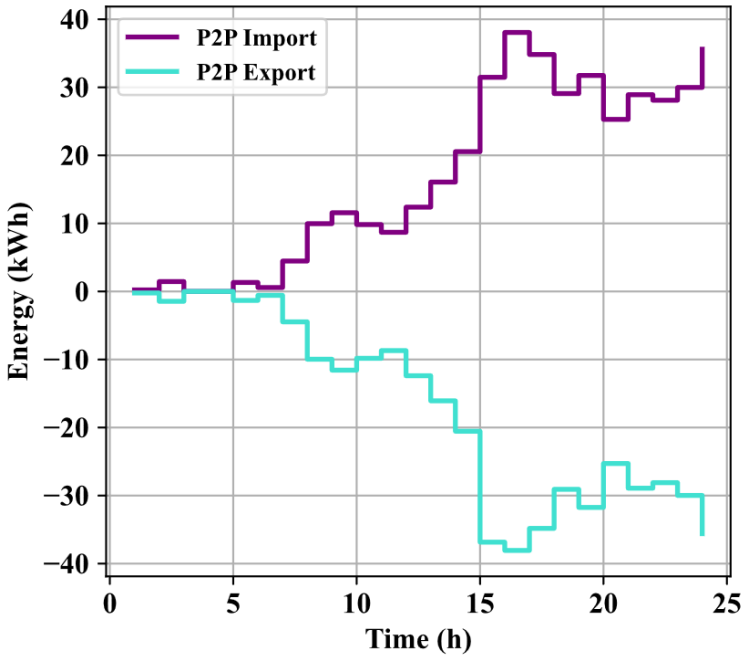

Fig. 5. Hourly P2P import and export energy flows under Scenario 1 (positive: import; negative: export).

Fig. 6 shows the hourly energy balance across all resources. During off-peak periods, the grid and DG mainly supply the load, while PV and wind contributions increase during daylight hours. In the evening, as renewable generation decreases, increased demand is addressed by distributed generation operation, grid imports, and synchronized discharging from the energy-storage system and EV. P2P trading enhances local load fulfillment. The system effectively supports the 250-kW evening peak; however, this results in increased distributed generation usage and corresponding emissions due to a lack of demand flexibility.

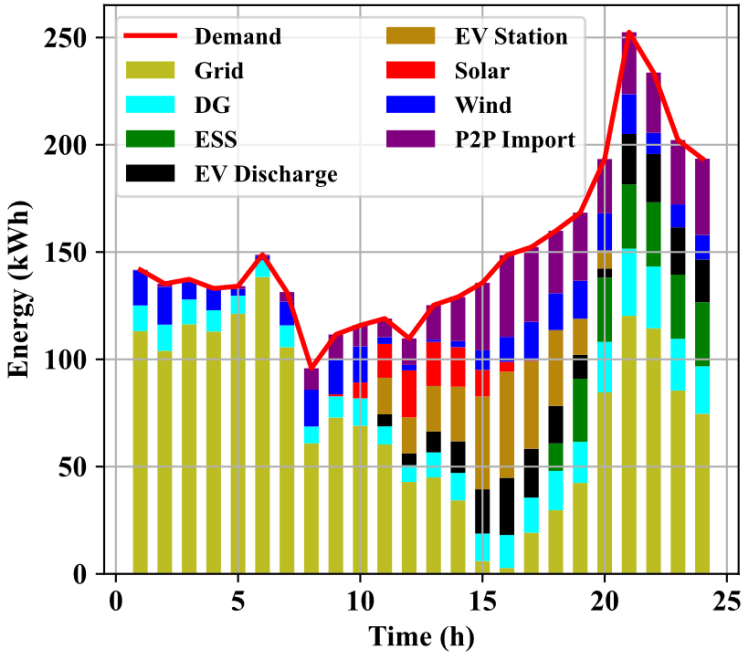

Fig. 6. Hourly community energy balance over 24 hours under scenario 1.

Fig. 7 shows a Pareto front that highlights the correlation between total emissions and social welfare, and also points out the trade-off that appears in Scenario 1. The selected operational solution achieves a social welfare of \$6721.449 and a total emission level of 3255.172 kg CO_2. This point is located near the optimal area of the frontier, indicating a balance between ecological effects and economic advantages. Welfare-oriented dispatch enhances distributed power generation and grid participation, while emission-focused operation emphasizes renewable sources and storage discharges. The curved shape of the frontier gives an opportunity to validate an anticipated inverse relation and shows the strength of the optimization model.

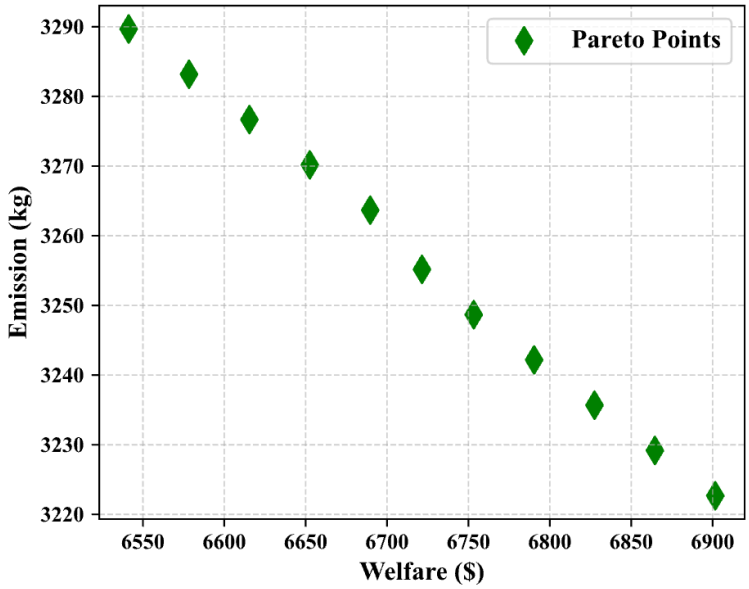

Fig. 7. Pareto front trade-off between total emission and welfare for Scenario 1.

In a non-DR configuration, system flexibility is often obtained with energy storage, EV discharging, and P2P transactions. Although these mechanisms can partly remedy a lack of demand adaptability, they bring more emissions and less social welfare when compared to the upcoming demand-responsive scenario.

4.4. Scenario 2: With Demand Response

Fig. 8 depicts the P2P import and export flows over a 24-hour period for the DR scenario. Imports and exports are balanced, affirming energy conservation within the trading network. In contrast to the non-DR scenario, import peaks are reduced and occur earlier, while mid-day exports rise due to demand transitioning to solar-rich hours. The more uniform patterns suggest that DR participation corrects the load curve and diminishes reliance on evening-peak trading.

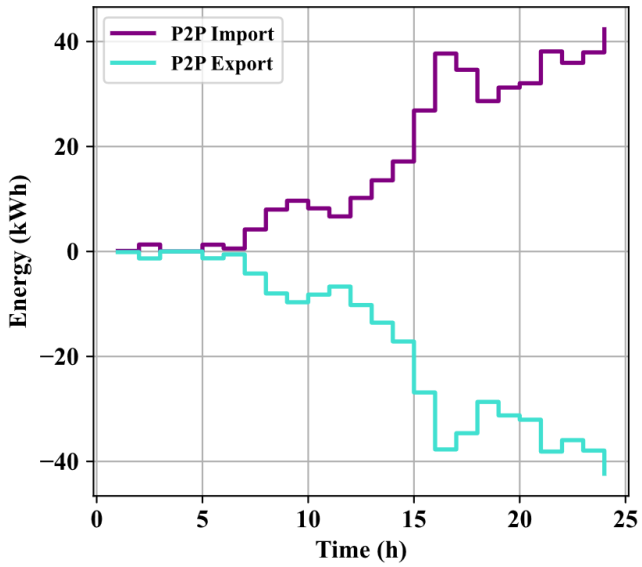

Fig. 8. P2P import and export profiles over 24 hours under Scenario 2 (positive: import; negative: export).

Fig. 9 illustrates the associated energy balance across all sources. DR redistributes usage to periods plentiful in renewable energy, enhancing the utilization of PV and wind resources while reducing the operation of DG. Grid imports decrease, and the energy-storage system (ESS) undergoes a reduction in charge–discharge cycles. EV discharging has an alignment more highly with demand during the evening, which indicates improved coordination among flexible loads and the distributed resources.

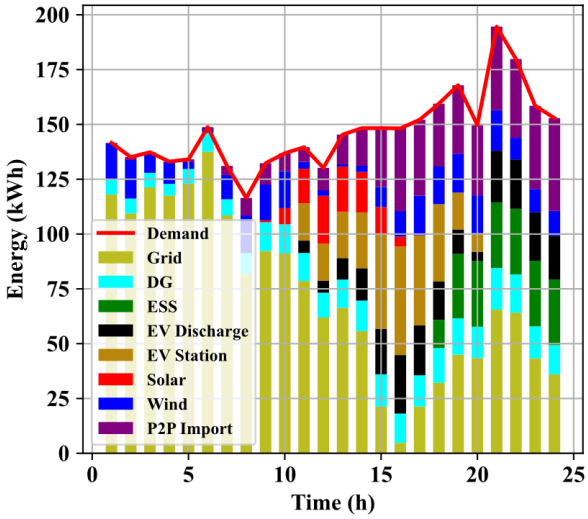

Fig. 9. Hourly energy community balance over 24 h in Scenario 2 with DR.

Fig. 10 depicts the Pareto front concerning emissions and welfare under DR. Opposed to Scenario 1, both metrics exhibit favorable shifts: emissions decline from 3255.172 to 2692.027 kg CO_2 (approximately 17.3% reduction), while welfare decreases from \$6721.449 to \$5741.462 (approximately 14.6% lower) as DR mandates load redistribution towards cleaner yet less economically advantageous schedules. The more streamlined and compact frontier shows improved stability and decreased decision uncertainty, attributed to reduced dependence on distributed generation and increased renewable integration. Social welfare is evaluated as the net welfare defined in Eq. (36), i.e., the economic terms (consumer surplus and system profit) minus the comfort-disutility associated with load adjustment. Therefore, the observed welfare decrease under DR is economically consistent when the additional disutility induced by load redistribution outweighs the operational savings from lower-emission dispatch; furthermore, incentive and P2P settlement payments are treated as internal transfers within the community and thus do not inflate welfare, and comfort loss is accounted only once through the disutility term.

A comparative benchmark has been performed between NSGA-II and a Multi-Objective Particle Swarm Optimizer (MOPSO) on the same optimization model, constraints, input data, and time. Both algorithms have been run with the same stopping criterion (200 iterations) and identical feasibility handling. Performance was evaluated using the hypervolume (HV) indicator computed at each iteration. Fig. 11 reports the mean HV trajectory over 30 independent runs together with the 95% confidence interval of the mean. The results show faster HV improvement and a higher final HV for NSGA-II relative to MOPSO, indicating more effective convergence toward the Pareto-optimal set under the adopted settings.

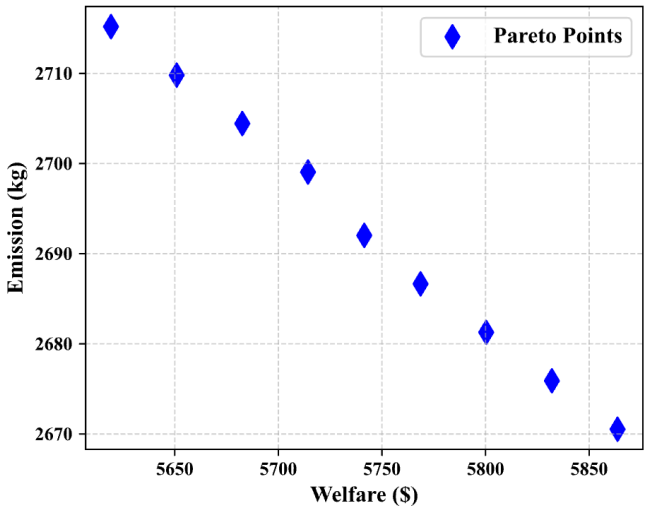

Fig. 10. Pareto front emission–welfare trade-off under Scenario 2 with DR.

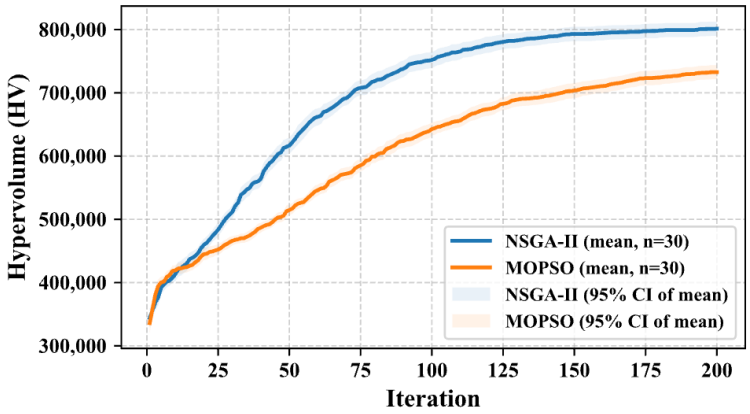

Fig. 11. HV convergence of NSGA-II and MOPSO under identical settings.

The DR-enabled system significantly reduces emissions and enhances resource synergy; however, it results in a moderate decrease in welfare. By supporting temporal flexibility and also matching demand to a renewable generation, DR allows an enhanced sustainability plus grid efficiency compared to a non-DR setup. Table 4 shows forecasting accuracy for machine learning models that are being used for predicting the demand, PV, and wind. The Root Mean Square Error (RMSE) and Mean Absolute Error (MAE) values remain within acceptable boundaries for every variable. This signifies reliable short-term forecasting performance. Demand prediction attained the minimal RMSE of 0.205, indicating robust temporal learning of consumption patterns. PV and wind forecasts exhibit marginally elevated errors (RMSE ≈ 0.235–0.253) attributable to the stochastic characteristics of weather-dependent generation. These metrics confirm that the models generate accurately precise inputs for emission-welfare optimization and scenario assessments.

Table 4. Prediction accuracy metrics for demand, PV, and wind forecasts.

Train	**MAE**	**RMSE**
Demand	0.2015	0.2054
PV	0.2322	0.2355
Wind	0.1992	0.2531
Test	**MAE**	**RMSE**
Demand	0.2553	0.3394
PV	0.2708	0.3463
Wind	0.2492	0.3196

5. Conclusion

This paper introduces a peer-to-peer energy trading framework that combines coordinated demand response and multi-objective optimization through NSGA-II with data-driven forecasting to account for temporal variability in PV, wind, and load profiles. By combining an RNN-based forecast with a probabilistic uncertainty representation, the framework enables uncertainty-aware scheduling under variable renewable conditions. The case-study results indicate that coordinated demand response can improve environmental performance, reducing emissions by approximately 17%, while preserving social welfare at an acceptable level for the studied community. The Pareto-front analysis emphasizes the trade-off between welfare and emissions and demonstrates the framework's capacity to identify balanced operating points. Overall, the proposed technique provides a structured decision-making basis for P2P market operation in decentralized energy communities, with potential for broader applicability subject to further validation on additional case studies and real-world datasets.

Future research will focus on real-time adaptive control and multi-community coordination, including deep reinforcement learning for dynamic decision-making under uncertainty.

Acknowledgement

N/A

Authorship Contribution Statement

Xiao Cao: Conceptualization, Writing-Original draft preparation, Project administration.

Data Availability

Available upon request.

Conflicts of Interest

The authors hereby declare that no conflicts of interest exist in relation to the publication of this manuscript.

References

[1] N. Shaukat, M.R. Islam, M.M. Rahman, B. Khan, B. Ullah, S.M. Ali, A. Fekih, "Decentralized, democratized, and decarbonized future electric power distribution grids: A survey on the paradigm shift from the conventional

power system to microgrid structures," IEEE Access, vol. 11, pp. 60957–60987, 2023.

[2] M. Cavus, "Advancing power systems with renewable energy and intelligent technologies: A comprehensive review on grid transformation and integration," Electronics (Basel), vol. 14, no. 6, p. 1159, 2025.

[3] Y. Wu, Y. Wu, H. Cimen, J. C. Vasquez, and J. M. Guerrero, "Towards collective energy community: Potential roles of microgrid and blockchain to go beyond P2P energy trading," Applied Energy, vol. 314, p. 119003, 2022.

[4] E. Ejuh Che, K. Roland Abeng, C. D. Iweh, G. J. Tsekouras, and A. Fopah-Lele, "The impact of integrating variable renewable energy sources into grid-connected power systems: Challenges, mitigation strategies, and prospects," Energies (Basel), vol. 18, no. 3, p. 689, 2025.

[5] C. Medina, C. R. M. Ana, and G. González, "Transmission grids to foster high penetration of large-scale variable renewable energy sources—A review of challenges, problems, and solutions," International Journal of Renewable Energy Research, vol. 12, no. 1, pp. 146–169, 2022.

[6] D. Stanelyte, N. Radziukyniene, and V. Radziukynas, "Overview of demand-response services: A review," Energies (Basel), vol. 15, no. 5, p. 1659, 2022.

[7] Z. Ji, X. Liu, and D. Tang, "Game-theoretic applications for decision-making behavior on the energy demand side: A systematic review," Protection and Control of Modern Power Systems, vol. 9, no. 2, pp. 1–20, 2024.

[8] H. El Hafdaoui, A. Khallaayoun, and S. AlMajeed, "Controlled non-dominated sorting genetic algorithms for multi-objective optimal design of standalone and grid-connected renewable energy systems in integrated energy sectors," IEEE Access, early access, 2025.

[9] S. S. Leal and P. E. M. de Almeida, "Traffic light optimization using non-dominated sorting genetic algorithm (NSGA-II)," Scientific Reports, vol. 13, no. 1, p. 15550, 2023.

[10] S. T. Alharbi, "Multi-objective evolutionary algorithms in waste disposal systems: A comprehensive review of applications, case studies, and future directions," Computers, vol. 14, no. 8, p. 316, 2025.

[11] P. M. J. Ganesh, B. M. Sundaram, P. K. Balachandran, and M. A. A. M. Zainuri, "Syner-dandelion optimization integrated temporal recurrent transformer network for accurate energy load forecasting in IoT-smart grids," IEEE Internet of Things Journal, early access, 2025.

[12] D. Feng and J. Zhang, "Integrated energy forecasting and blockchain-based trading using hybrid LSTM and HHO for distributed consumer systems," IEEE Transactions on Consumer Electronics, early access, 2025.

[13] N. Uddin, Y. Wu, M. S. Islam, and K. M. Zakaria, "An optimized decentralized peer-to-peer energy trading system for smart grids incorporating uncertain renewable energy sources through fuzzy optimization," Electric Power Systems Research, vol. 238, p. 111154, 2025.

[14] P. Xie and C. Li, "Dynamic modeling and optimization of energy storage in peer-to-peer energy trading systems," Eksploatacja i Niezawodność – Maintenance and Reliability, vol. 27, no. 2, 2025.

[15] T. Al-Abri, A. Onen, M. W. Khan, R. Al-Abri, A. Al-Rawahi, and S. Al-Saad, "Catalyzing sustainable energy transition in Oman: A peer-to-peer energy trading model with integrated GHG emission mitigation strategies," IEEE Access, early access, 2025.

[16] X. Dai and K. Batool, "Optimizing multi-objective design, planning, and operation for sustainable energy sharing districts considering electrochemical battery longevity," Renewable Energy, vol. 229, p. 120705, 2024.

[17] M. Yavuz and Ö. C. Kivanç, "Optimization of a cluster-based energy management system using deep reinforcement learning without affecting prosumer comfort: V2X technologies and peer-to-peer energy trading," IEEE Access, vol. 12, pp. 31551–31575, 2024.

[18] N. Karthik, A. Rajagopalan, M. Bajaj, P. Medhi, R. Kanimozhi, V. Blazek, L. Prokop, "Chaotic self-adaptive sine cosine multi-objective optimization algorithm to solve microgrid optimal energy scheduling problems," Scientific Reports, vol. 14, no. 1, p. 18997, 2024.

[19] Y. Zhou, "A dynamic self-learning grid-responsive strategy for battery sharing economy—Multi-objective optimisation and posteriori multi-criteria decision making," Energy, vol. 266, p. 126397, 2023.

[20] S. Akiyama and N. Shinomiya, "A multi-objective optimization method for efficiency and fairness in P2P electricity trading model," in 2023 International Technical Conference on Circuits/Systems, Computers, and Communications (ITC-CSCC), 2023, pp. 1–4.

[21] J. Gao, Z. Shao, F. Chen, Y. Chen, Y. Lin, and H. Deng, "Distributed robust operation strategy of multi-microgrid based on peer-to-peer multi-energy trading," IET Energy Systems Integration, vol. 5, no. 4, pp. 376–392, 2023.

[22] V. Lokesh and A. Q. H. Badar, "Optimal sizing of RES and BESS in networked microgrids based on proportional peer-to-peer and peer-to-grid energy trading," Energy Storage, vol. 5, no. 7, p. e464, 2023.

[23] A. Ramadan, M. Ebeed, S. Kamel, M. I. Mosaad, and A. Abu-Siada, "Technoeconomic and environmental study of multi-objective integration of PV/wind-based DGs considering uncertainty of system," Electronics (Basel), vol. 10, no. 23, p. 3035, 2021.

[24] Z. Belboul, M. Khelifi, A. Chouder, and K. Kara, "Multiobjective optimization of a hybrid PV/Wind/Battery/Diesel generator system integrated in microgrid: A case study in Djelfa, Algeria," Energies (Basel), vol. 15, no. 10, p. 3579, 2022.

[25] M. K. Deshmukh and S. S. Deshmukh, "Modeling of hybrid renewable energy systems," Renewable and Sustainable Energy Reviews, vol. 12, no. 1, pp. 235–249, 2008.

[26] H. Ding, Y. Xu, B. Chew Si Hao, Q. Li, and A. Lentzakis, "A safe reinforcement learning approach for multi-energy management of smart home," Electric Power Systems Research, vol. 210, p. 108120, 2022, doi: 10.1016/j.epsr.2022.108120.

[27] L. A. Soriano, M. Avila, P. Ponce, J. de Jesús Rubio, and A. Molina, "Peer-to-peer energy trades based on multi-objective optimization," International Journal of Electrical Power & Energy Systems, vol. 131, p. 107017, 2021, doi: 10.1016/j.ijepes.2021.107017.

[28] M. R. Elshenawy, A. Mohamed, A. A. Ali, and M. A. Mosa, "Two-stage multi-objective framework for optimal operation of modern distribution network considering demand response program," Scientific Reports, vol. 15, no. 1, p. 989, 2025.

[29] S. Sheikhmemari, "Recurrent neural network controller for linear and nonlinear systems," in International Conference on Intelligent and Fuzzy Systems, Springer, 2022, pp. 752–760.

[30] M. Ahmad, R. A. Al-Mansob, A. B. Bin Ramli, F. Ahmad, and B. J. Khan, "Unconfined compressive strength prediction of stabilized expansive clay soil using machine learning techniques," Multiscale and Multidisciplinary Modeling, Experiments and Design, vol. 7, no. 1, pp. 217–231, 2024.

[31] H. Wei, Y. Chen, and Q. Wang, "Enhance solar power generation using advanced computational techniques for improved forecast accuracy and efficiency," International Journal of Renewable Energy Research, vol. 15, no. 2, pp. 416–433, 2025.

[32] C. Sun and Y. Che, "Monte Carlo-based prediction of electric vehicle charging load and coupling mechanisms of multiple information sources," International Journal of Renewable Energy Research, vol. 15, no. 1, pp. 42–55, 2025.